Materials Research. 2025; 28: e20250430
DOI: https://doi.org/10.1590/1980-5373-MR-2025-0430

Surface Functionalization of Natural Short Diss (Ampelodesmos mauritanicus) Fiber with Graphene Nanoplatelets for Advanced Applications: Structural, Thermal, and Morphological Characterization

Hakim Gouigah[a], Nouredine Bouzegzi[a], Ismail Daoud[a]*, Maria Teresa de Miguel[b], Mohamed Kenane[a], Said Abdi[a], Francisco Javier Pérez[b]

[a]University of Sciences and Technology Houari Boumediene, Laboratory of Science and Materials Engineering, Bab Ezzouar, 16111, Algiers, Algeria.
[b]Universidad Complutense de Madrid, Facultad de Ciencias Químicas, Research Group of Surface Engineering and Nanostructured Materials, 28040, Madrid, Spain.

Received: April 26, 2025; Revised: July 26, 2025; Accepted: August 21, 2025

Understanding interfacial interactions is a key to enhancing composite performance. This study aims to investigate the structural, thermal, and morphological properties of short Diss (Ampelodesmos mauritanicus) fiber (SDF) functionalized with graphene nanoplatelets (GNPs). The diss fibers were first extracted and then alkali-treated with 4% (w/v) NaOH, while the graphene nanoplatelets were sonicated. A functionalized short diss fibers-graphene nanoplatelets (SDFGNPs) was prepared using a simple mixing method. The results clearly demonstrated strong adhesion of graphene to the fiber surface, as confirmed by electron microscope micrographs. This resulted in improved thermal stability of the fibers, as evidenced by T_{max} increasing from 343 °C to 353 °C, indicating a marked enhancement in thermal resistance, along with a notable 70.25% reduction in final accumulated weight loss. Furthermore, spectroscopic analysis revealed the absence of any chemical bonding, supporting the hypothesis that graphene nanoplatelets mechanically adhere to the fiber surface.

Keywords: *Natural Fiber, Diss, Graphene Nanoplatelets, Mixing Method, Functionalization.*

1. Introduction

The expanding use of biodegradable materials has become a global necessity and increasingly attracts interest for several reasons. Among these, the need to preserve and protect the environment has driven the continuous adoption of eco-friendly alternatives and valuing natural resources, such as natural fibers. The latter demonstrated an effective solution due to their various interesting properties including biodegradability, affordable cost, significantly reduced environmental impact, and their viability as alternatives to synthetic fibers. Consequently, research in this field is expanding rapidly, along with their growing application across various industries[1,2]. However, some fibers remain underexploited and have not been researched extensively, such as diss fiber.

Diss fiber is a species of plant widely found in the Mediterranean area. It is primarily composed of cellulose, lignin, hemicellulose, and extractable matter, with mass fractions of 45.2%, 15.6%, 26%, and 13.2%, respectively[3]. May and Moussa[4] conducted a detailed characterization of diss fibers using various analytical techniques. Their findings suggest that diss fibers represent a promising alternative to conventional non-wood raw materials, offering potential for sustainable applications. Recently, some works were achieved using diss fibers as reinforcement, in polymer matrix[5,6], and cement matrix[7]. In this regard, Nouri et al.[5] demonstrated that reinforcement with a 10% diss fiber mass loading improves the mechanical properties of the polypropylene (PP) biocomposite.

Natural fibers usually undergo chemical treatments, such as alkali treatment, to reduce their hydrophilicity, thereby enhancing their adhesion to the polymer matrix[8]. This, in turn, improves the overall performance of the composite. For example, the hardness of NaOH-treated Balanites aegyptiaca fiber (NBA) composites was investigated and compared to that of raw Balanites aegyptiaca fiber (RBA) composites. The treated composites exhibited higher hardness values, which increased with increasing fiber weight loading[9]. Moreover, thermal analysis was conducted to evaluate the suitability of alkali-treated Cordia dichotoma fiber compared to untreated fiber. The results indicated that the treated fiber exhibited greater thermal stability, supporting its use as a reinforcement material in composites processed at temperatures not exceeding 290 °C[10]. In another work, Reddy et al.[11] reported that polyester composites reinforced with alkali-treated Tapsi fibers demonstrated superior mechanical properties compared to those with untreated fibers. As a natural lignocellulosic fiber, diss is often treated chemically, particularly through alkali treatment, to modify

*e-mail: ismail.daoud@usthb.edu.dz
Associate Editor: Sandro Amico.
Editor-in-Chief: Luiz Antonio Pessan.

its structural and interfacial properties. In this regard, research conducted by Achour et al.[12] indicates that treating diss fibers with 1%, 2%, and 3% NaOH for 30 minutes leads to a significant increase in the crystallinity index by 7%, 8%, and 13%, respectively. Furthermore, Remila et al.[6] reported that incorporating 20%.wt of treated diss fiber in poly (3-hydroxybutyrate-co-3-hydroxyvalerate) (PHBV) biocomposite enhances their mechanical and thermal properties.

On the other hand, the use of nanomaterial additives has continued to grow across various domains thanks to their exceptional properties, for example the high specific surface area. As a result, their application as nanofillers has attracted significant attention from researchers aiming to enhance the performance of polymer-based composites. Graphene, a widely recognized nanomaterial, is a two-dimensional (2D) structure consisting of a single layer of carbon atoms structured in a hexagonal arrangement[13]. In general, graphene can be categorized based on the number of its constituent layers, as follows: single-layer, bilayer, few-layer, and nanoplatelet forms (GNPs)[14].

In several studies, the effect of graphene nanoplatelets (GNPs) have been investigated across a wide range of research fields, notably as nanofiller in polymer matrix[15]. Srivastava et al.[16] examined the influence of graphene nanoplatelets coating content on the mechanical properties of carbon fiber/epoxy composites. The obtained results revealed a significant enhancement of 20% in flexural modulus with the incorporation of 0.4 wt.% graphene nanoplatelets. Moreover, a study was conducted to investigate the incorporation of 1 wt.% graphene nanoplatelets (GNPs) into polyaniline (PANI). The resulting PANI/GNPs nanocomposites exhibited a 100% improvement in electrical conductivity compared to graphene-free PANI[17]. Additionally, Zailan et al.[18] demonstrated that adding 2 wt.% of graphene nanoplatelets (GNPs) along with 3 wt.% of polyanilines (PANi) to the (TPNR/PANi/GNPs) nanocomposite led to a 62.8% increase in tensile strength and a 151.8% enhancement in Young's modulus. Other research[19] highlights the effects of graphene on the performance of polymer-based composites reinforced with natural flax fibers. Their findings indicate that graphene significantly enhances matrix-fiber interfacial adhesion, leading to improved composite properties. Boudjellal et al.[20] prepared a hybrid material based on Alfa fibers/graphene nanoplatelets. The resulting composite showed uniform graphene nanoplatelets deposition on the surface of Alfa fiber, along with improved thermal stability, highlighting its potential for advanced applications. In another study, functionalized graphene nanoplatelets were incorporated into polylactic acid/liquid natural rubber (PLA/LNR) nanocomposites. The results indicated that both ADA-functionalized GNPs (GNP-A) and TX100-functionalized GNPs (GNP-T) exhibited improved dispersion within the nanocomposite compared to unfunctionalized GNPs, which contributed to enhanced mechanical properties[21].

This work aims to prepare a functionalized filler/fiber material by combining short diss fibers with graphene nanoplatelets (SDFGNPs) using a mixing method. The structural, thermal, and morphological properties of the prepared material were investigated through multiple characterization techniques. The findings can provide insights into the interface mechanisms, which could enhance future applications and aid in selecting the appropriate choice for composites materials reinforced with natural diss fibers.

2. Materials and Methods

2.1. Materials

Diss plant was harvested from Algeria in North Africa. Graphene nanoplatelets (GNPs) were obtained from NANOGRAFI (Turkey) with the following specifications: specific surface area of 320 m^2/g, 99.9% purity, diameter of 1.5 µm, and an average thickness of 3 nm. Figure 1 presents an overview of the GNPs used in this work. Figure 1a displays TEM micrograph of GNPs at low magnification. As shown, a clear contrast in darkness is observed, resulting from the overlapping of the planar GNPs layers. On the other hand, Figure 1b exhibits GNPs at high magnification, illustrating a stack of layers with a thickness of 4.71 nm and 2.63 nm, confirming the technical specifications provided by the supplier. Figure 1c shows the XPS survey spectra of GNPs, with two peaks corresponding to binding energies of C1s at 284 eV and O1s at 532 eV. These peaks reveal a high carbon content of 95.3% and low oxygen content of 4.7%, with a C/O ratio of 20.27. The low oxygen content likely originates from slight oxidation during purification or limited exposure to ambient moisture[22].

2.2. Preparation of short diss fibers (SDF)

The diss stems were separated from the plant and cut into short segments, averaging 3 mm in length, followed by mechanical grinding. The resulting short diss fibers (SDF)

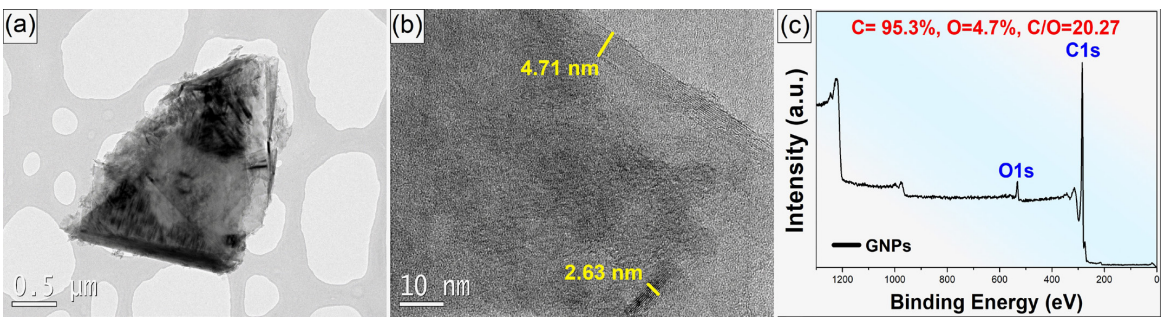

Figure 1. TEM micrographs and XPS analysis of GNPs, (a) low magnification (b) high magnification and (c) XPS survey spectra.

were subjected to Soxhlet extraction using a toluene-ethanol (62/38% v/v) mixture for 6 hours to eliminate extractable substances. Finally, the extracted SDF underwent drying at 65 °C until complete evaporation.

2.3. Alkali treatment

An alkali treatment was carried out to eliminate the non-cellulosic components and impurities. The SDF were immersed in a 4% (w/v) sodium hydroxide (NaOH) solution for a total duration of 6 h, conducted in three equal cycles of 2 hours each[23]. Camargo et al.[24] reported that adequate alkali treatments enhance cellulose crystallinity, whereas higher concentration cause excessive delignification, weakening or damaging the fibers. After each cycle, the SDF were thoroughly washed with distilled water. A neutralization step was then performed using acetic acid (CH_3COOH) until a neutral pH was reached. Finally, the treated SDF were dried at 65 °C for 6 h.

2.4. Preparation of functionalized filler/fiber (SDFGNPs)

Initially, GNPs were dispersed into ethanol at a concentration of 1 mg/ml, followed by a sonication for 2 h. Thereafter, a functionalized filler/fiber was prepared by a simple mixing method. For instance, to prepare SDFGNPs containing 0.1 g of SDF, a quantity of 0.1 g of GNPs is required, which is equivalent to 100 ml of dispersed GNPs solution. The mixture was then magnetically stirred at 300 rpm for 2 hours at 65 °C. Afterward, the short diss fibers/graphene nanoplatelets (SDFGNPs) was dried at 65 °C for 6 hours to remove any remaining ethanol. A schematic illustration detailing the sequential steps involved in the preparation of SDFGNPs is depicted in Figure 2.

2.5. Methods

Transmission electron microscopy (TEM) analysis was undertaken using a JEOL-JEM-2100 (JEOL Ltd., Tokyo, Japan) operated with a LaB6 electron gun at 200 kV and equipped with a CCD camera (Orious SC1000). X-ray photoelectron spectroscopy (XPS) analysis was achieved using an XPS ESCALAB 250XI Spectrometer (Thermo Fisher Scientific Inc, MA, USA), with a monochromatic Al-Kα radiation source at emission energy of 1486.6 eV. Scanning electron microscopy (SEM) analysis was examined with the aid of a JEOL JSM-7610FPlus (JEOL Ltd., Tokyo, Japan) with Schottky-type field emission (S-FEG). Raman spectroscopy analysis was accomplished using a RENISHAW Spectrometer at room temperature. An operating power of 25 mW and a 633 nm laser excitation were used. The spectra were plotted between 500 and 3500 cm^{-1}. Fourier Transform Infrared Spectroscopy (FTIR) analysis was obtained employing a Jasco FT/IR-4X Spectrometer. The range and resolution scan parameters were 4000 to 400 cm^{-1} and 4 cm^{-1}, respectively. Thermal behavior was investigated through Thermogravimetric analysis (TGA) and Differential Scanning Calorimetry (DSC). TGA analysis was performed via an SDT Q600 (TA Instruments) with a heating rate of 10°C/min, from room temperature to 550 °C under a nitrogen environment. DSC analysis was carried out under a nitrogen atmosphere by means of Q20 instrument (TA Instruments). The temperature ranged from 25 °C to 400 °C, with a heating rate of 10 °C/min. X-ray diffraction (XRD) analysis was assessed with a PANalytical X-pert PRO-MRD diffractometer equipped with CuKα radiation (λ = 1.54060 Å). The scan was operated at 40 kV/15 mA, and 2θ sweeps from 10° to 70° with a step size of 0.03°.

3. Results and Discussion

3.1. Morphological analysis (SEM)

Figure 3 displays the SEM micrographs of untreated SDF, treated SDF, GNPs, and SDFGNPs. As shown in

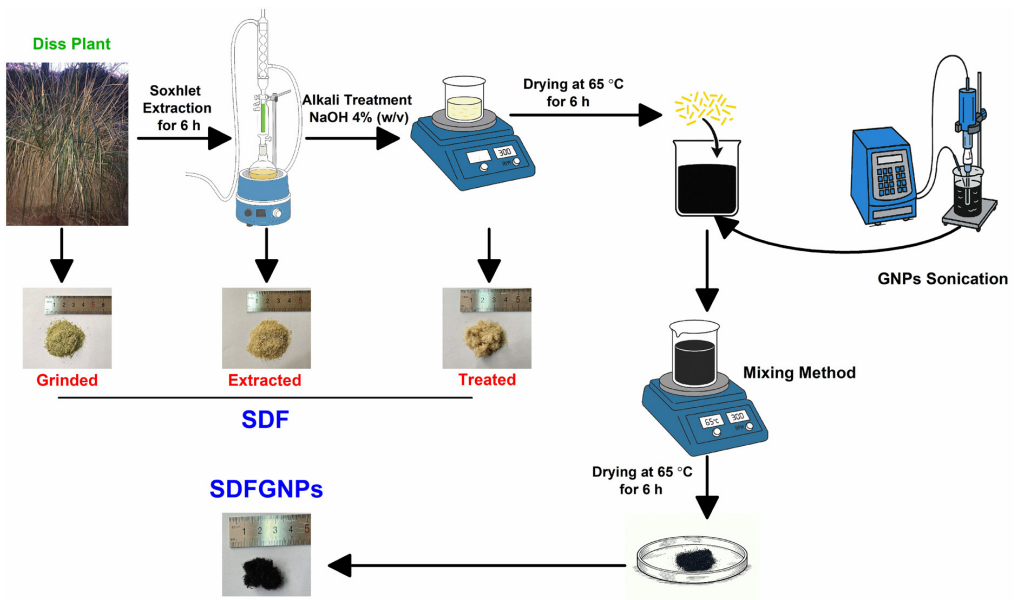

Figure 2. Schematic illustration of SDFGNPs preparation steps.

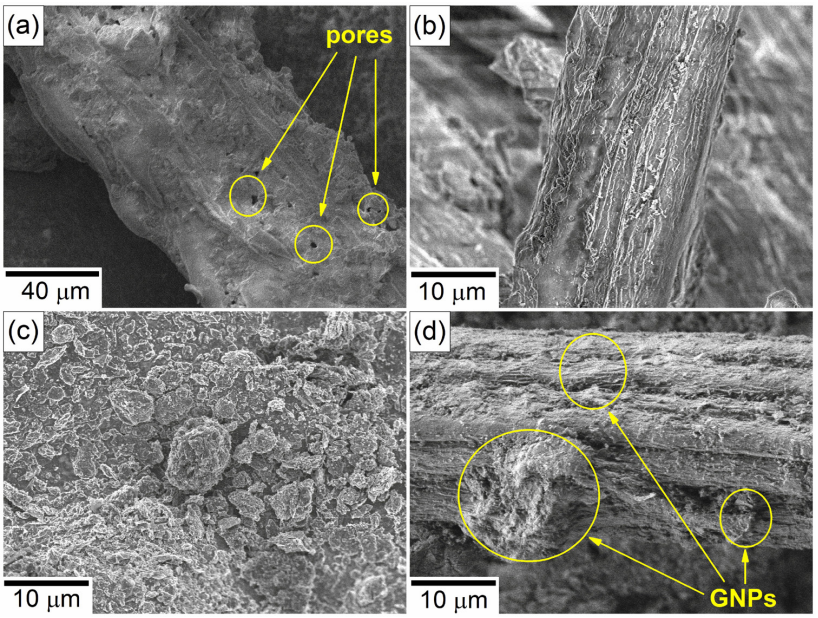

Figure 3. SEM micrographs of (a) untreated SDF, (b) treated SDF, (c) GNPs, and (d) SDFGNPs.

Figure 3a, the longitudinal view of the raw diss fiber reveals a highly rough and uneven surface with visible impurities, attributed to the presence of non-cellulosic compounds such as hemicellulose and lignin. In addition, waxes and some pores are also distinguishable on their external surface. After alkali treatment, Figure 3b clearly shows a remaining rough but cleaner surface of the SDF, resulting from the effective removal of non-cellulosic constituents. Figure 3c illustrates the morphology of GNPs highlighting their varying sizes. In the case of SDFGNPs, as demonstrated in Figure 3d, the distribution of GNPs on the SDF fibers surface can be clearly seen. The GNPs are firmly adhered to the SDF due to the roughness of the fiber surface and irregularities, covering the entire surface and forming laminated layers. A similar phenomenon was observed by Boudjellal et al.[20], reporting a uniform distribution of GNPs on the surface of Alfa Fiber (AF) and effective adhesion between the AF and GNPs. Indeed, the formation of ripples and wrinkles resulting from the edge instability in GNPs, could influence their attachment on the SDF surface[25]. Additionally, the GNPs form stacked clusters due to interactions between the layers of the nanoplatelets through van der Waals forces and π-π stacking[26].

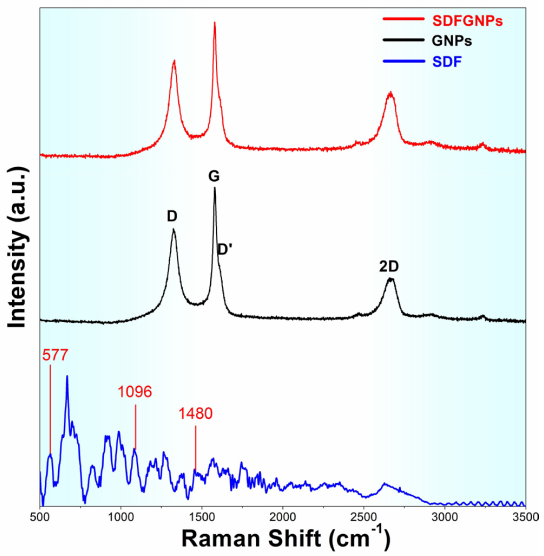

Figure 4. RAMAN spectra of SDF, GNPs, and SDFGNPs.

3.2. RAMAN spectroscopy

The Raman spectra of SDF, GNPs, and the SDFGNPs are shown in Figure 4, displaying four distinct peaks at 1330 cm^{-1}, 1580 cm^{-1}, 1615 cm^{-1}, and 2670 cm^{-1} in both GNPs and the SDFGNPs. The positions of these peaks remain consistent, suggesting that the GNPs structure has not been altered. The D peak at 1330 cm^{-1} is an indicative of defects in the structure of GNPs[27]. The in-plane vibrational mode arising from the excitation of C–C bonds is represented by the G band at 1580 cm^{-1} [28]. Moreover, a slight shoulder D′ peak observed at 1615 cm^{-1} further indicates defects associated with elastic and inelastic phonon scattering[29]. Additionally, the 2D band, observed at approximately 2670 cm^{-1}, is commonly considered to be a second-order scattering process related to the D peak[30]. On the other hand, peaks appearing at approximately 577 cm^{-1}, 1096 cm^{-1} , and 1480 cm^{-1} in the SDF spectrum correspond to vibrational modes associated with the cellulosic structure of natural fibers, as reported in the literature[31,32]. However, these peaks have completely vanished in the SDFGNPs spectrum. This phenomenon is attributed to the barrier effect caused by the coverage of the fiber surface by graphene nanoplatelets, which effectively decreases the cellulose signals during Raman analysis. A similar phenomenon was reported by da Silveira et al.[33], where the characteristic cellulose peaks disappeared in hemp fibers coated with graphene oxide.

3.3. Fourier transform infrared spectroscopy analysis (FTIR)

The FTIR spectra of GNPs, SDF, and SDFGNPs are shown in Figure 5. As can be seen in GNPs spectrum, a weak absorption band at 3322 cm^{-1} corresponds to –OH stretching vibrations, suggesting the presence of hydroxyl groups. A distinct peak around 1532 cm^{-1} is attributed to aromatic C=C bonds, representing the skeletal vibrations of the hexagonal graphitic backbone[34]. Additionally, two absorption bands at approximately 2840 cm^{-1} and 2912 cm^{-1} are associated with C–H stretching vibrations. The characteristic peaks observed at 1112 cm^{-1} and 1664 cm^{-1} are linked to C–O and C–C stretching vibrations. Meanwhile, the existence of oxidized or hydroxyl functional groups in GNPs is likely a consequence of oxidation during the purification process or exposure to atmospheric moisture[22].

A comparison of the FTIR spectra for SDF and the SDFGNPs shows that their characteristic peaks remain largely unchanged, suggesting that there is no chemical interaction between SDF and GNPs. This probably indicates that the GNPs are mechanically adhered to the SDF surface. As expected for natural fibers, the FTIR spectrum of SDF exhibits a peak at 895 cm^{-1}, characteristic of cellulose β-bonds[35]. Moreover, a sharp band recorded at 1026 cm^{-1} is associated to the stretching vibration of C–OH bond, characteristic of polysaccharides[36]. Additionally, two peaks were identified at 1102 cm^{-1} and 1158 cm^{-1} highlights characteristic features of cellulose, ascribed to the C–C cycle of the carbohydrate backbone and to the C–O–C stretching vibration of the glycosidic bonds, respectively[37]. Moreover, two peaks were observed at 1315 cm^{-1}, assigned to the wagging vibration of cellulose, and at 1365 cm^{-1} ascribed to the hydroxyl group (OH) deformation[38].

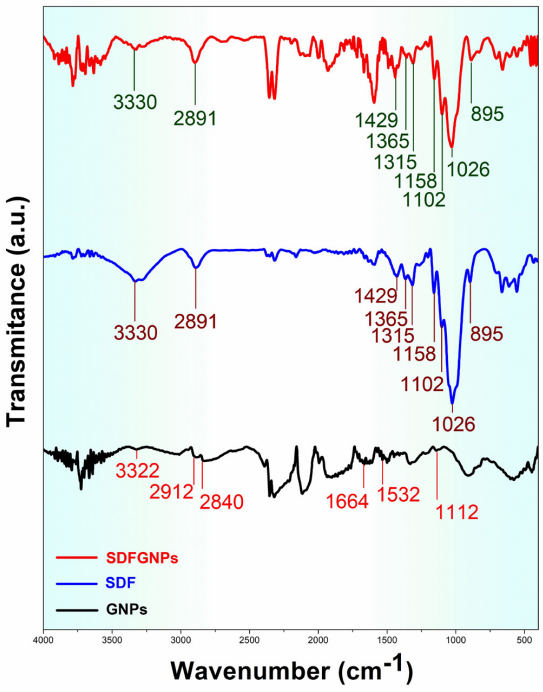

Figure 5. FTIR spectra of GNPs, SDF, and SDFGNPs.

The absorption peak at 1429 cm^{-1} is attributed to the CH_2 groups bending vibration in cellulose[39]. Another peak appears at 2891 cm^{-1}, related to the methyl stretching vibration. In this regard, Gwon et al.[36] reported that the absorbance peak at 2902 cm^{-1} shifted to 2894 cm^{-1} and became sharper after NaOH treatment, compared to the untreated wood, suggesting a transformation in the cellulose crystal structure after alkali treatment. Furthermore, the absorption band at 3330 cm^{-1}, corresponding to the hydroxyl groups in cellulose and water within the fibers[40], became less broad and attenuated after the addition of GNPs. Sarker et al.[41] observed a similar phenomenon in jute fibers coated with graphene flakes.

3.4. X-Ray diffraction analysis (XRD)

The XRD patterns of GNPs, SDF, and SDFGNPs are shown in Figure 6. The SDF pattern exhibits a prominent peak at 2θ = 22.48°, characteristic of the cellulose (002) diffraction plane. In addition, two weaker peaks at 2θ = 15.62° and 34.56°, attributed to the (110) and (004) planes, respectively. The last observed planes are typically associated with the presence of amorphous cellulose[39]. Furthermore, the GNPs exhibits a sharp peak at 2θ = 26.41°, corresponds to the graphitic (002) plane attributed to the interlayer d-spacing of 0.34 nm[42]. Moreover, smaller peaks are observed at 2θ = 43.14°, 2θ = 44.34°, and 2θ = 54.51°, corresponding to the graphitic (100), (101) and (004) plane reflections, respectively[43]. For the SDFGNPs, the XRD pattern shows the characteristic peaks of both SDF and GNPs, with no new peaks detected, suggesting that there is no interaction between the GNPs and the SDF, which is consistent with the FTIR analysis results.

3.5. Thermogravimetric analysis (TGA) and derivative thermogravimetry (DTG)

The TGA and DTG curves of GNPs, SDF, and the SDFGNPs are shown in Figure 7. As observed in Figure 7a, GNPs display a stable thermal behavior with a mass loss of 3.6%. Furthermore, both SDF and the SDFGNPs exhibit a similar decomposition pattern, though with different mass loss and residual weight percentages. Notably, the decomposition of SDF and SDFGNPs occurs in three distinct stages: Stage I (room temperature – 220 °C), Stage II (220 – 400 °C), and Stage III (400 – 550 °C).

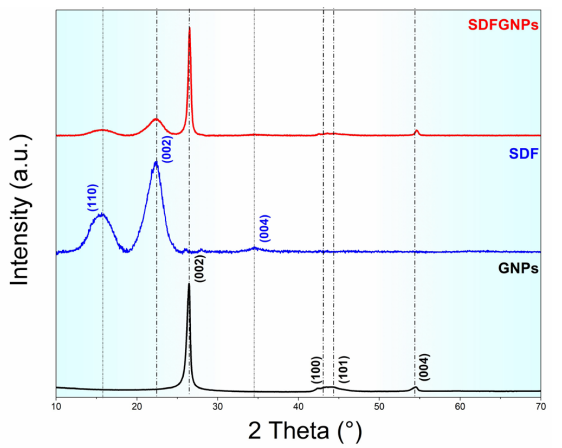

Figure 6. XRD patterns of (a) GNPs, (b) SDF, and (c) SDFGNPs.

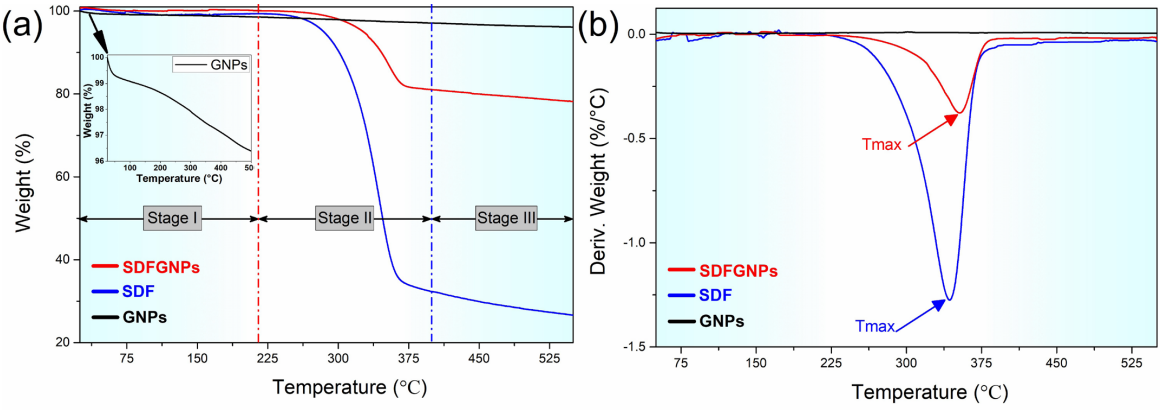

Figure 7. (a) TGA and (b) DTG curves of GNPs, SDF, and SDFGNPs.

In stage I, a minor weight loss is observed up to 220 °C. This phenomenon is attributed to the evaporation of moisture within the fiber and the decomposition of hemicellulose[35]. By the end of this stage, the total mass loss is approximately 0.5%, 1.5%, and 1% for GNPs, SDF, and SDFGNPs, respectively. The subsequent stage, considered the most critical in the thermal decomposition process, involves significant degradation primarily due to the breakdown of the cellulose component. It is evident that the onset temperature (T_{onset}) of SDF is 14 °C lower than that of the SDFGNPs, with values of 303 °C and 317 °C, respectively. A similar decrease is observed in weight loss as well. By the end of this stage, the maximum degradation for SDF reaches 68%, while the SDFGNPs shows a degradation of 19%. Concurrently, the DTG curves reveal a marked degradation rate during this stage (as seen in Figure 7b), where the T_{max} values are 343 °C and 353 °C for SDF, and SDFGNPs, respectively. This shift indicates an improvement of 2.9% in thermal resistance. This behavior aligns with the depolymerization of cellulose. The final stage (400 – 550 °C) shows a slow decomposition, attributed to the breakdown of SDF towards the end of the thermal degradation process. The accumulated weight loss at the end of this stage is 73.3% for SDF and 21.8% for the SDFGNPs, indicating an improvement of 70.25% in weight loss. In this stage, the decomposition is attributed to the degradation of cellulose and lignin. However, lignin, known for its high thermal resistance, undergoes degradation over a broad temperature range (from 220 to 550 °C) due to its complex aromatic structure[44]. GNPs notably enhance the thermal stability and resistance to thermal degradation of the SDFGNPs compared to SDF. This improvement is due to the barrier function of GNPs, which contributes to delaying the thermal decomposition of the SDF components.

3.6. Differential scanning calorimetry (DSC)

The DSC curves of GNPs, SDF, and SDFGNPs are presented in Figure 8. A broad endothermic peak is observed around 153 °C and 145 °C, with the corresponding enthalpies of ΔH = 146 J/g and ΔH = 300 J/g, reflecting the maximum energy needed for the evaporation of absorbed moisture from SDF and SDFGNPs, respectively. Similarly, an endothermic transition for GNPs appears at approximately 128 °C, with ΔH = 128 J/g. Additionally, the SDF and

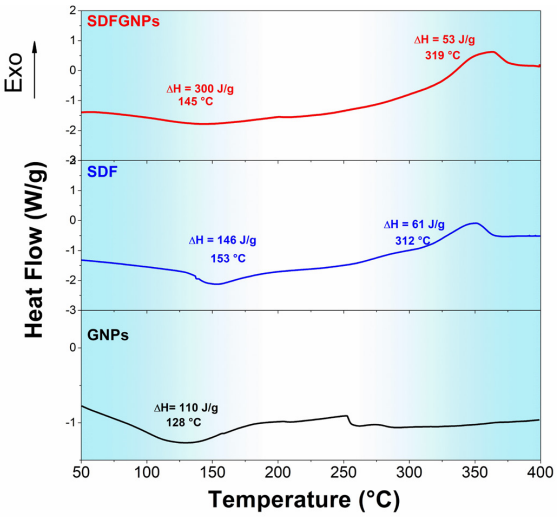

Figure 8. DSC curves of GNPs, SDF, and SDFGNPs.

SDFGNPs exhibit a second endothermic peak at 312 °C and 319 °C, with associated enthalpy values of ΔH = 61 J/g and ΔH = 53 J/g, respectively. This peak correlates with the one observed in the DTG curves, indicating the degradation of fiber components such as cellulose and lignin at these temperatures. Interestingly, the addition of GNPs results in a shift of the decomposition peak to a higher temperature in the SDFGNPs. Meanwhile, a decrease in the enthalpy required for decomposition is observed in the SDFGNPs, supporting the hypothesis that the thermal stability is improved due to the barrier effect of graphene. Kim and Lee[45] observed a similar trend in electrically heated textiles coated with a high-content GNP/PVDF-HFP composite.

4. Conclusions

Short diss fibers functionalized with graphene nanoplatelets (SDFGNPs) was successfully prepared by mixing method. The effect of GNPs on structural, thermal, and morphological properties of SDFGNPs was investigated. The findings of this research can be summarized as follows: SEM analysis clearly demonstrated the adhesion of graphene nanoplatelets

onto the surface of the diss fibers, effectively covering them. This adhesion was confirmed to be purely mechanical, as no new chemical bonds were formed, as evidenced by the FTIR analysis. Additionally, no new peaks appeared in the XRD and Raman spectra. The TGA results highlighted the significant effect of the graphene nanoplatelets in enhancing the thermal stability of the diss fibers, acting as a barrier that delays degradation. The DSC analysis revealed two endothermic peaks, corresponding to moisture evaporation and fiber degradation, with shifted temperatures after fiber functionalization. The developed functionalized material, due to its improved properties, holds strong potential for advanced applications such as insulating panels, smart textiles, and reinforced polymer composites.

5. References

1. Palanisamy S, Vijayananth K, Murugesan TM, Palaniappan M, Santulli C. The prospects of natural fiber composites: a brief review. Int J Lightweight Mater Manuf. 2024;7(4):496-506. http://doi.org/10.1016/j.ijlmm.2024.01.003.
2. Madhusudhan Reddy B, Venkata Mohana Reddy Y, Chandra Mohan Reddy B, Meenakshi Reddy R. Mechanical, morphological, and thermogravimetric analysis of alkali-treated Cordia-Dichotoma natural fiber composites. J Nat Fibers. 2020;17(5):759-68. http://doi.org/10.1080/15440478.2018.1534183.
3. Bekkouche SR, Benzerara M, Zada U, Muhammad G, Ali Z. Use of eco-friendly materials in the stabilization of expansive soils. Buildings. 2022;12(10):1770. http://doi.org/10.3390/buildings12101770.
4. May C, Moussa A. Chemical and structural analysis of lignocellulosic biomass of Ampelodesmos mauritanicus (DISs) and Stipa tenacissima. Wood Res. 2018;63:699-712.
5. Nouri M, Tahlaiti M, Grondin F. Effect of chemical and physical treatments on mechanical properties of diss fibers-based biocomposites materials. J Nat Fibers. 2023;20(1):2128148. http://doi.org/10.1080/15440478.2022.2128148.
6. Remila B, Zembouai I, Zaidi L, Alane A, Kaci M, Kervoelen A, et al. Investigations on structure and properties of poly (3-hydroxybutyrate-co-3-hydroxyvalerate) (PHBV) reinforced by diss fibers: effect of various surface treatments. Ind Crops Prod. 2024;221:119302. http://doi.org/10.1016/j.indcrop.2024.119302.
7. Sellami A, Bouayad D, Benazzouk A, Amziane S, Merzoud M. Study of toughness and thermal properties of bio-composite reinforced with diss fibers for use as an insulating material. Energy Build. 2022;276:112527. http://doi.org/10.1016/j.enbuild.2022.112527.
8. Karthi N, Kumaresan K, Sathish S, Gokulkumar S, Prabhu L, Vigneshkumar N. An overview: natural fiber reinforced hybrid composites, chemical treatments and application areas. Mater Today Proc. 2020;27:2828-34. http://doi.org/10.1016/j.matpr.2020.01.011.
9. Reddy BM, Reddy RM, Reddy PV, Nittala NAP, Bandhu D. Effect of alkali treatment on mechanical properties and morphology of the Balanites aegyptiaca composite. Proc Inst Mech Eng, C J Mech Eng Sci. 2023;238(11):5077-86. http://doi.org/10.1177/09544062231217596.
10. Reddy BM, Reddy YVM, Reddy BCM, Kumar GS, Reddy PV, Raghavendra Rao H. A study on mechanical, structural, morphological, and thermal properties of raw and alkali treated Cordia dichotoma-polyester composite. Polym Compos. 2021;42(1):309-19. http://doi.org/10.1002/pc.25826.
11. Meenakshi Reddy R, Mohana Krishnudu D, Madhusudhan Reddy B, Venkateshwar Reddy P. Effect of Alkali treatment on mechanical properties of tapsi fiber reinforced polyester composites. In: Vijayaraghavan L, Reddy K, Jameel Basha S, editors. Emerging trends in mechanical engineering. Singapore: Springer Singapore; 2020. http://doi.org/10.1007/978-981-32-9931-3_9.
12. Achour A, Ghomari F, Belayachi N. Properties of cementitious mortars reinforced with natural fibers. J Adhes Sci Technol. 2017;31(17):1938-62. http://doi.org/10.1080/01694243.2017.1290572.
13. Laraba SR, Luo W, Rezzoug A, Zahra Q, Zhang S, Wu B, et al. Graphene-based composites for biomedical applications. Green Chem Lett Rev. 2022;15(3):724-48. http://doi.org/10.1080/17518253.2022.2128698.
14. Kumar N, Salehiyan R, Chauke V, Botlhoko OJ, Setshedi K, Scriba M, et al. Top-down synthesis of graphene: a comprehensive review. FlatChem. 2021;27:100224. http://doi.org/10.1016/j.flatc.2021.100224.
15. Flaifel MH, Shahdan D, Mhareb MHA, Ahmad SH, Alghamdi AAA, Alajerami YS, et al. Unveiling enhanced properties of sustainable hybrid multifunctional graphene nanoplatelets incorporated polylactide/liquid natural rubber/polyaniline bio-nanocomposites for advanced radiation and particle shielding applications. J Mater Sci. 2024;59(30):13824-42. http://doi.org/10.1007/s10853-024-10028-5.
16. Srivastava AK, Gupta V, Yerramalli CS, Singh A. Flexural strength enhancement in carbon-fiber epoxy composites through graphene nano-platelets coating on fibers. Compos, Part B Eng. 2019;179:107539. http://doi.org/10.1016/j.compositesb.2019.107539.
17. Razak JA, Khalid NA, Hasib H, Mahamood MA, Ismail MM, Mohamad N, et al. Electrical conductivity and Antenna properties of polyaniline filled GNPs nanocomposites. Malaysian Journal on Composites Science and Manufacturing. 2021;4(1):11-27. http://doi.org/10.37934/mjcsm.4.1.1127.
18. Zailan FD, Chen RS, Ahmad SH, Flaifel MH, Shahdan D, Wan NWB, et al. Synergistic improvement of mechanical, electrical and thermal properties by graphene nanoplatelets in polyaniline incorporated rubbery thermoplastic composites. J Mater Res Technol. 2024;28:4097-109. http://doi.org/10.1016/j.jmrt.2024.01.018.
19. Sarker F, Karim N, Afroj S, Koncherry V, Novoselov KS, Potluri P. High-performance graphene-based natural fiber composites. ACS Appl Mater Interfaces. 2018;10(40):34502-12. http://doi.org/10.1021/acsami.8b13018. PMid:30222307.
20. Boudjellal A, Trache D, Bekhouche S, Khimeche K, Razali MS, Guettiche D. Preparation and characterization of Alfa fibers/graphene nanoplatelets hybrid for advanced applications. Mater Lett. 2021;289:129379. http://doi.org/10.1016/j.matlet.2021.129379.
21. Nurul AMA, Ahmad S, Chen RS, Shahdan D, Flaifel MH, Omar A. Assessment of mechanical and electrical performances of polylactic acid/liquid natural rubber/graphene platelets nanocomposites in the light of different graphene platelets functionalization routes. Macromol Chem Phys. 2021;222(19):2100185. http://doi.org/10.1002/macp.202100185.
22. Bello RH, Coelho LAF, Becker D. Role of chemical funcionalization of carbon nanoparticles in epoxy matrices. J Compos Mater. 2017;52(4):449-64. http://doi.org/10.1177/0021998317709082.
23. Zergane H, Abdi S, Xu H, Hemming J, Wang X, Willför S, et al. Ampelodesmos mauritanicus a new sustainable source for nanocellulose substrates. Ind Crops Prod. 2020;144:112044. http://doi.org/10.1016/j.indcrop.2019.112044.
24. Camargo MM, Taye EA, Judith A Roether DTR, Boccaccini A. A review on natural fiber-reinforced geopolymer and cement-based composites. Materials (Basel). 2020;13(20):4603. http://doi.org/10.3390/ma13204603. PMid:33081091.
25. Deng S, Berry V. Wrinkled, rippled and crumpled graphene: an overview of formation mechanism, electronic properties, and applications. Mater Today. 2016;19(4):197-212. http://doi.org/10.1016/j.mattod.2015.10.002.
26. Chiou Y-C, Olukan T, AlMahri M, Apostoleris H, Chiu CH, Lai CY, et al. Direct measurement of the magnitude of the van der waals interaction of single and multilayer graphene.

Langmuir. 2018;34(41):12335-43. http://doi.org/10.1021/acs.langmuir.8b02802. PMid:30244581.
27. Paton KR, Despotelis K, Kumar N, Turner P, Pollard AJ. On the use of Raman spectroscopy to characterize mass-produced graphene nanoplatelets. Beilstein J Nanotechnol. 2023;14:509-21. http://doi.org/10.3762/bjnano.14.42. PMid:37152472.
28. Jiang Z, Sevim O, Ozbulut O. Mechanical properties of graphene nanoplatelets-reinforced concrete prepared with different dispersion techniques. Constr Build Mater. 2021;303:124472. http://doi.org/10.1016/j.conbuildmat.2021.124472.
29. Guerra V, Wan C, Degirmenci V, Sloan J, Presvytis D, Watson M, et al. Characterisation of graphite nanoplatelets (GNP) prepared at scale by high-pressure homogenisation. J Mater Chem C Mater Opt Electron Devices. 2019;7(21):6383-90. http://doi.org/10.1039/C9TC01361J.
30. Zhang B, Chen T. Study of ultrasonic dispersion of graphene nanoplatelets. Materials (Basel). 2019;12(11):1757. http://doi.org/10.3390/ma12111757. PMid:31151185.
31. Jähn A, Schröder MW, Füting M, Schenzel K, Diepenbrock W. Characterization of alkali treated flax fibres by means of FT Raman spectroscopy and environmental scanning electron microscopy. Spectrochim Acta A Mol Biomol Spectrosc. 2002;58(10):2271-9. http://doi.org/10.1016/S1386-1425(01)00697-7. PMid:12212753.
32. Agarwal U, Ralph S. Raman spectra of delignified plant fibers: exploring the impact of Xylan's presence on the spectral features of cellulose. Fibers (Basel). 2023;12(1):5. http://doi.org/10.3390/fib12010005.
33. da Silveira PHPM, Ribeiro MP, Silva TT, Lima AM, Lemos MF, Oliveira AGBAM, et al. Effect of alkaline treatment and graphene oxide coating on thermal and chemical properties of hemp (Cannabis Sativa L.) fibers. J Nat Fibers. 2022;19(15):12168-81. http://doi.org/10.1080/15440478.2022.2053265.
34. Dericiler K, Alishah HM, Bozar S, Güneş S, Kaya F. A novel method for graphene synthesis via electrochemical process and its utilization in organic photovoltaic devices. Appl Phys, A Mater Sci Process. 2020;126(11):904. http://doi.org/10.1007/s00339-020-04091-3.
35. Nouri M, Griballah I, Tahlaiti M, Grondin F, Beaugrand J. Plant extraction and physicochemical characterizations of untreated and pretreated diss fibers (Ampelodesmos mauritanicus). J Nat Fibers. 2021;18(8):1083-93. http://doi.org/10.1080/15440478.2019.1687062.
36. Gwon JG, Lee SY, Doh GH, Kim JH. Characterization of chemically modified wood fibers using FTIR spectroscopy for biocomposites. J Appl Polym Sci. 2010;116(6):3212-9. http://doi.org/10.1002/app.31746.
37. Mosiewicki MA, Marcovich NE, Aranguren MI. Characterization of fiber surface treatments in natural fiber composites by infrared and Raman spectroscopy. In: Zafeiropoulos N.E., editor Interface engineering of natural fibre composites for maximum performance. Woodhead Publishing; 2011. p. 117-45. http://doi.org/10.1533/9780857092281.1.117.
38. Touati Z, de Hoyos-Martinez PL, Belhaneche-Bensemra N, Charrier- El Bouhtoury F. Influence of different diss fiber treatments over the properties of poly propylene/recycled and regenerated low density polyethylene based biocomposites. J Polym Environ. 2021;29(1):291-303. http://doi.org/10.1007/s10924-020-01877-7.
39. Touati Z, Boulahia H, Belhaneche-Bensemra N, Massardier V. Modification of diss fibers for biocomposites based on recycled low-density polyethylene and polypropylene blends. Waste Biomass Valoriz. 2019;10(8):2365-78. http://doi.org/10.1007/s12649-018-0225-x.
40. Remila B, Zembouai I, Zaidi L, Kaci M, Kervoelen A, Bruzaud S. Surface treatment effects on morphological and property enhancements of poly (3-hydroxybutyrate-co-3-hydroxyvalerate)/Diss fibers (Ampelodesmos mauritanicus) biocomposites. J Polym Compos. 2024;46(3):2404-19. http://doi.org/10.1002/pc.29113.
41. Sarker F, Potluri P, Afroj S, Koncherry V, Novoselov KS, Karim N. Ultrahigh performance of nanoengineered graphene-based natural jute fiber composites. ACS Appl Mater Interfaces. 2019;11(23):21166-76. http://doi.org/10.1021/acsami.9b04696.
42. Kumar V, Kumar A, Lee D-J, Park S-S. Estimation of number of graphene layers using different methods: a focused review. Materials (Basel). 2021;14(16):4590. http://doi.org/10.3390/ma14164590. PMid:34443113.
43. Batakliev T, Georgiev V, Kalupgian C, Muñoz PAR, Ribeiro H, Fechine GJM, et al. Physico-chemical characterization of PLA-based composites holding carbon nanofillers. Appl Compos Mater. 2021;28(4):1175-92. http://doi.org/10.1007/s10443-021-09911-0.
44. Xiang A, Ebdon JR, Horrocks AR, Kandola BK. On the utility of thermogravimetric analysis for exploring the kinetics of thermal degradation of lignins. Bioresour Technol Rep. 2022;20:101214. http://doi.org/10.1016/j.biteb.2022.101214.
45. Kim H, Lee S. Characterization of electrical heating textile coated by graphene nanoplatelets/PVDF-HFP composite with various high graphene nanoplatelet contents. Polymers (Basel). 2019;11(5):928. http://doi.org/10.3390/polym11050928. PMid:31137888.

Data Availability

The entire dataset supporting the results of this study was published in the article itself.